Deep Variational Quantum Eigensolver: A Divide-And-Conquer Method for Solving a Larger Problem with Smaller Size Quantum Computers

Keisuke Fujii,[1,2,3,*] Kaoru Mizuta,[4] Hiroshi Ueda,[2,5,6] Kosuke Mitarai,[1,2,6] Wataru Mizukami,[2,6] and Yuya O. Nakagawa[7]

[1] *Graduate School of Engineering Science, Osaka University, 1-3 Machikaneyama, Toyonaka, Osaka 560-8531, Japan*

[2] *Center for Quantum Information and Quantum Biology, Institute for Open and Transdisciplinary Research Initiatives, Osaka University, Japan*

[3] *RIKEN Center for Quantum Computing (RQC), Wako, Saitama 351-0198, Japan*

[4] *Department of Physics, Kyoto University, Kyoto 606-8502, Japan*

[5] *Computational Materials Science Research Team, RIKEN Center for Computational Science (R-CCS), Kobe 650-0047, Japan*

[6] *JST, PRESTO, 4-1-8 Honcho, Kawaguchi, Saitama 332-0012, Japan*

[7] *QunaSys Inc., Aqua Hakusan Building 9F, 1-13-7 Hakusan, Bunkyo, Tokyo 113-0001, Japan*

(Received 2 October 2020; revised 25 January 2022; accepted 16 February 2022; published 21 March 2022)

We propose a divide-and-conquer method for the quantum-classical hybrid algorithm to solve larger problems with small-scale quantum computers. Specifically, we concatenate a variational quantum eigensolver (VQE) with a reduction in the system dimension, where the interactions between divided subsystems are taken as an effective Hamiltonian expanded by the reduced basis. Then the effective Hamiltonian is further solved by the VQE, which we call *deep VQE*. Deep VQE allows us to apply quantum-classical hybrid algorithms on small-scale quantum computers to large systems with strong intrasubsystem interactions and weak intersubsystem interactions, or strongly correlated spin models on large regular lattices. As proof-of-principle numerical demonstrations, we use the proposed method for quasi-one-dimensional models, including one-dimensionally coupled 12-qubit Heisenberg antiferromagnetic models on kagome lattices as well as two-dimensional Heisenberg antiferromagnetic models on square lattices. The largest problem size of 64 qubits is solved by simulating 20-qubit quantum computers with a reasonably good accuracy approximately a few %. The proposed scheme enables us to handle the problems of > 1000 qubits by concatenating VQEs with a few tens of qubits. While it is unclear how accurate ground-state energy can be obtained for such a large system, our numerical results on a 64-qubit system suggest that deep VQE provides a good approximation (discrepancy within a few percent) and has room for further improvement. Therefore, deep VQE provides us a promising pathway to solve practically important problems on noisy intermediate-scale quantum computers.

DOI: 10.1103/PRXQuantum.3.010346

I. INTRODUCTION

Quantum computers are expected to solve certain problems, such as prime factorization [1], quantum chemistry calculations [2,3], and linear algebraic processes (matrix inversion) [4–6], exponentially faster than classical computers. By virtue of the extensive engineering effort paid for the realization of quantum computers, we now have a quantum computer that is already intractable for classical computers to simulate, namely quantum-computing supremacy [7]. However, the size of current quantum computers is too small to implement fault-tolerant quantum computation, where quantum information is protected by quantum error correction. Such a transitional period is called the noisy intermediate-scale quantum (NISQ) technology era [8]. Since the task of demonstrating quantum-computing supremacy [7,9,10] is not useful for practical applications, our next milestone in the NISQ era is to demonstrate the advantage of using NISQ devices for those problems that expand our scientific frontier.

* fujii@qc.ee.es.osaka-u.ac.jp

To this end, a significant amount of NISQ-oriented algorithms have emerged recently. Among them, the variational quantum eigensolver (VQE) [11] has attracted much attention because of its notable feature that directly exploits quantum states generated on a quantum computer for practical problems such as quantum chemistry calculations. While the objective of the original method was to find an approximate ground state of a quantum system, it has widely been extended since its first appearance. Researchers have proposed various techniques, for example, to construct approximate excited states [12–16], investigate nonequilibrium steady states in open quantum systems [17], and calculate energy derivatives [18–20].

However, there are several serious problems in applications of real quantum devices: noise is too high to perform deeper quantum computation, and the number of qubits is too small to handle practically interesting problems. Though we can resolve these by further experimental efforts in the future, for the meantime we should develop algorithmic approaches to relax the hardware limitation. Regarding the noise issue, error-mitigation techniques [21–26], has been investigated actively, and its experimental validity has already been demonstrated [27]. To relax the hardware size or connectivity limitation, virtual quantum gates have been introduced to decompose a large quantum circuit into smaller ones with quasiprobability sampling [28–30]. There are several techniques for reducing the required number of qubits, for example, by exploiting symmetries of a target system [31,32] or by so-called active-space approximation [12,33–35].

For quantum chemical calculations that are considered a promising application of NISQ, various divide-and-conquer (DC) techniques have been developed. Say, a density-matrix DC approach or a fragmentation method is widely used to perform large-scale molecular simulations [36,37]. These methods are employed with density-functional theory for weakly correlated systems. Meanwhile, another set of methods, such as the cluster mean-field theory [38–40], multilayer multiconfiguration time-dependent Hartree (ML MCTDH) [41,42], active-space decomposition (ASD) techniques [43–45], quasi-complete-active-space (QCAS) [46], the renormalization exciton model (REM) [47,48], and the n-body Tucker method [49,50], exist for quantum many-body systems with strong correlations in each subsystem and weak interactions between subsystems. This is by no means an exhaustive list, but the diversity and active development of DC methods reflect their importance in classical computing. NISQ has a severe limit on the number of available qubits considering the number of orbitals of a molecule. It is, therefore, highly desirable to develop a DC method designed in the framework of the quantum-classical hybrid algorithm.

Here, we introduce a general framework for implementing a DC method on the quantum-classical hybrid algorithm, which allows us to handle larger problems by diving them into small pieces so that NISQ devices can solve practically important large problems. It should be noted that while the use of DC techniques for the VQE has been explored in Refs. [51,52], where the authors proposed to combine existing DC techniques in the field of quantum chemistry [36,37,53], this work provides a more general technique applicable to any quantum system consisting of subsystems with weak intersubsystem interaction but strong intrasubsystem interaction. To investigate the properties of such a system, we utilize multiple small-scale quantum computers that are connected via classical computers. We divide the system into small subsystems, each of which is solved, as the first step, by using VQE neglecting intersubsystem interactions. The resultant approximated ground state is further used to generate a basis with reduced degrees of freedom to estimate an effective Hamiltonian including the intersubsystem interactions neglected in the first step. We concatenate VQE to solve the effective Hamiltonian, which we call *deep VQE*. In a sense, this scheme can be viewed as real-space renormalization using actual quantum devices.

We perform extensive numerical simulation on Heisenberg antiferromagnetic models with frustration as proof-of-principle demonstrations of deep VQE. A quasi-one-dimensional system with 48 qubits in total can be tackled with 12-qubit quantum computers. For a two-dimensional system, we apply deep VQE for up to 8×8 Heisenberg antiferromagnetic model on the square lattice using 16 or 20 qubit quantum computers. As seen later, we successfully obtain a lower ground-state energy than the energy calculated solely on the subsystems, which approaches the exact one. Deep VQE will be a powerful approach to solving practically important problems on a quantum computer with a limited number of qubits.

II. DEEP VQE

A. Divide-and-conquer method for VQE

Let us consider a Hamiltonian H, which can be decomposed into a sum of subsystem Hamiltonian H_i acting only on the ith subsystem and interaction terms V_{ij} acting on subsystems i and j [see Fig. 1(a)]:

$$H = \sum_i H_i + \sum_{ij} V_{ij}. \tag{1}$$

Suppose we have N subsystems, each of which consists of n qubits. Let M be the number of qubits required to describe the full Hamiltonian H, that is, $M = nN$. The situation that we expect in this work is as follows: each subsystem can be described by several tens to hundreds of qubits being subject to a strong intrasubsystem interaction, and these subsystems interact weakly with each

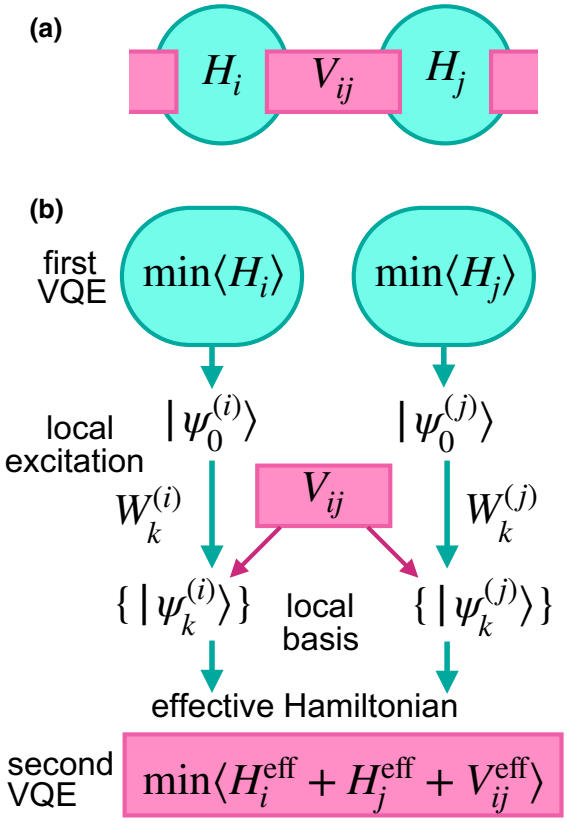

FIG. 1. (a) The system consists of subsystems of Hamiltonian H_i, each of which interact with each other by intersubsystem interaction V_{ij}. (b) To solve the system depicted in (a), we first construct an approximate ground state $|\psi_0^{(i)}\rangle$ of each H_i with VQE (the first VQE). Then we form a basis set by applying excitation operators on $|\psi_0^{(i)}\rangle$. Using the basis, we can construct an effective Hamiltonian, which gives better approximation of the ground state.

other, forming a larger system including thousands of qubits in total. There are indeed many such systems at the molecular level, such as molecular aggregates, molecular crystals, and dendrimers. Among those systems, this method would be suitable for describing singlet fission systems for organic light-emitting diodes (OLEDs) [54] and solar cells [55], or natural light-harvesting systems [56].

Our idea here is to decompose such a problem into smaller problems. As the first step, each subsystem Hamiltonian H_i is solved by the conventional VQE with neglecting the intersubsystem interactions, which we call the first VQE below. The qubits that are engaged in the intersubsystem interactions are called a boundary of the subsystem. The first VQE provides us a state close to the ground state of H_i,

$$|\psi_0^{(i)}\rangle = U_i(\vec{\theta}^{(i),*})|0^n\rangle, \tag{2}$$

where $U_i(\vec{\theta})$ is a parameterized unitary circuit with parameters $\vec{\theta}$ designed for H_i, and

$$\vec{\theta}^{(i),*} \equiv \arg\min_{\vec{\theta}^{(i)}} \langle 0^n|U_i(\vec{\theta}^{(i)})^\dagger H_i U_i(\vec{\theta}^{(i)})|0^n\rangle. \tag{3}$$

Hereafter we refer to $|\psi_0^{(i)}\rangle$ as a local ground state.

As the second step, we generate a K-dimensional local basis $\{|\psi_k^{(i)}\rangle\}_{k=1}^K$ from the local ground state by

$$|\psi_k^{(i)}\rangle \equiv W_k^{(i)}|\psi_0^{(i)}\rangle, \tag{4}$$

where $\{W_k^{(i)}\}$ is a set of operators on subsystem i, and $W_1^{(i)}$ is chosen to be an identity operator. The operator $W_k^{(i)}$ $(k \neq 1)$ should be chosen to be a local excitation on a qubit at the boundary of the subsystem. Suppose the intersubsystem Hamiltonian is given by

$$V_{ij} = \sum_k v_k W_k^{(i)} W_k^{(j)}. \tag{5}$$

Then the state is spanned by a product of the local basis

$$\sum_k v_k \left(W_k^{(i)}|\psi_0^{(i)}\rangle\right)\left(W_k^{(j)}|\psi_0^{(j)}\rangle\right) = V_{ij}|\psi_0^{(i)}\rangle|\psi_0^{(j)}\rangle, \tag{6}$$

i.e., an entangled state with respect to the local bases, contributes at least as a leading-order correction of the perturbation theory with a weak intersubsystem interaction V_{ij}. When the interaction term has a symmetry like a Heisenberg interaction, this entangled state recovers such a symmetry, even if it is broken in each subsystem. A concrete choice of $\{W_k^{(i)}\}$, as an example, is explained later.

The overlap between basis states can be estimated as an expectation value of ${W_k^{(i)}}^\dagger W_l^{(i)}$:

$$\langle\psi_k^{(i)}|\psi_l^{(i)}\rangle = \langle 0^n|U_i(\vec{\theta}^{(i),*})^\dagger {W_k^{(i)}}^\dagger W_l^{(i)} U_i(\vec{\theta}^{(i),*})|0^n\rangle. \tag{7}$$

Since $W_k^{(i)}$ is a local excitation, ${W_k^{(i)}}^\dagger W_l^{(i)}$ can be decomposed into a finite number of Hermitian operators. This allows us to calculate the overlap without any indirect measurement. Using the above inner product, we can also define the orthonormal basis $\{|\tilde{\psi}_k^{(i)}\rangle\}$ using a Gram-Schmidt process:

$$|\tilde{\psi}_k^{(i)}\rangle = \frac{1}{C_{k,i}}\left(|\psi_k^{(i)}\rangle - \sum_{l<k}\langle\tilde{\psi}_l^{(i)}|\psi_k^{(i)}\rangle|\tilde{\psi}_l^{(i)}\rangle\right), \tag{8}$$

where $C_{k,i}$ is the normalization factor, which can be calculated from $\{\langle\psi_k^{(i)}|\psi_l^{(i)}\rangle\}$. In this way, two bases are related

by a $K \times K$ matrix $P^{(i)}$,

$$|\tilde{\psi}_k^{(i)}\rangle = \sum_{k'=1}^{K} P_{kk'}^{(i)} |\psi_{k'}^{(i)}\rangle, \tag{9}$$

where the matrix element $P_{kk'}^{(i)}$ can be obtained from $\{\langle\psi_k^{(i)}|\psi_l^{(i)}\rangle\}$. Hereafter, we simply call this orthogonal basis a local basis.

At the third step, the effective Hamiltonian is constructed using the local basis. For the subsystem Hamiltonian, the matrix representation of the effective Hamiltonian with respect to the local basis is defined as follows:

$$(H_i^{\rm eff})_{kl} = \langle\tilde{\psi}_k^{(i)}|H_i|\tilde{\psi}_l^{(i)}\rangle. \tag{10}$$

Note that since the state that we can easily generate is $|\psi_k^{(i)}\rangle$, the effective Hamiltonian is calculated from

$$(\bar{H}_i^{\rm eff})_{kl} = \langle\psi_k^{(i)}|H_i|\psi_l^{(i)}\rangle \tag{11}$$

in actual calculations. Similarly to the previous case, $(\bar{H}_i^{\rm eff})_{kl}$ can be estimated with direct measurements by decomposing

$$W_k^{(i)\dagger} H_i W_l^{(i)} \tag{12}$$

into a linear combination of Hermitian operators, whose number is proportional to the number of terms in H_i. $(\bar{H}_i^{\rm eff})_{kl}$ and $(H_i^{\rm eff})_{kl}$ are related by

$$(H_i^{\rm eff})_{kl} = \sum_{k'l'} P^{(i)*}_{kk'} (\bar{H}_i^{\rm eff})_{k'l'} P^{(i)}_{ll'} = \left(P^{(i)*} \bar{H}_i^{\rm eff} P^{(i)T}\right)_{kl}, \tag{13}$$

where $*$ and T indicate complex conjugate and transpose, respectively.

In addition, we take the intersubsystem interactions, which are neglected in the first step. Their matrix representations are defined by using the associated local bases:

$$(V_{ij}^{\rm eff})_{kk'll'} = \langle\tilde{\psi}_k^{(i)}|\langle\tilde{\psi}_{k'}^{(j)}|V_{ij}|\tilde{\psi}_l^{(i)}\rangle|\tilde{\psi}_{l'}^{(j)}\rangle. \tag{14}$$

Recall that the interaction term V_{ij} defined in Eq. (5) is written as a sum of tensor product operators. Then it can be estimated by using an n-qubit quantum computer from

$$(V_{ij}^{\rm eff})_{kk'll'} = \sum_{\nu} v_\nu \langle\tilde{\psi}_k^{(i)}|W_\nu^{(i)}|\tilde{\psi}_l^{(i)}\rangle\langle\tilde{\psi}_{k'}^{(j)}|W_\nu^{(j)}|\tilde{\psi}_{l'}^{(j)}\rangle. \tag{15}$$

Note that it is enough to calculate the matrix elements independently on each subsystem. Similarly to the previous case, the effective intersubsystem Hamiltonian is calculated from expectation values obtained by $\{|\psi_k^{(i)}\rangle\}$ applying the linear transformation $P^{(i)}$. In this way, we now have an effective Hamiltonian $H^{\rm eff}$ of H,

$$H^{\rm eff} = \sum_i H_i^{\rm eff} + \sum_{ij} V_{ij}^{\rm eff}, \tag{16}$$

which acts on the K^N-dimensional system. For a fixed accuracy, this takes $O[\mathrm{poly}(M)K^4N]$ runs of quantum computers of n qubits, where $\mathrm{poly}(M)$ is responsible for counting the number of terms in H. The energy expectation value with respect to a product state of the local basis, $\bigotimes_{i=1}^N |\tilde{\psi}_0^{(i)}\rangle$, can be written as

$$H_{00}^{\rm eff} := \sum_i (H_i^{\rm eff})_{00} + \sum_{ij} (V_{ij}^{\rm eff})_{0000}, \tag{17}$$

which is the starting point of improving the ground-state energy in the proposed scheme.

As the fourth step, which is crucial in the proposed scheme, we use VQE again to find the ground state of the effective Hamiltonian. Suppose we have an m-qubit system, where m is chosen to be $m = N\lceil\log_2(K)\rceil$. The number of qubits is reduced from M to m. A parameterized quantum circuit $V(\vec{\phi})$ to generate an approximate ground state of $H^{\rm eff}$ is constructed appropriately so that $V(\vec{\phi})$ acts on K^N-dimensional subspace of the 2^m-dimensional Hilbert space. Then the expectation value of the effective Hamiltonian can be expressed as

$$\langle 0^m|V(\vec{\phi})^\dagger H^{\rm eff} V(\vec{\phi})|0^m\rangle, \tag{18}$$

which serves as the cost function of the second VQE. Note that if the ground-state energy is set to be negative, a parameterized quantum circuit acting fully on the m-qubit system finds the ground state in the K^N-dimensional subspace appropriately, simply by minimizing the energy expectation value.

The effective Hamiltonian $H^{\rm eff}$, which is described by $K \times K$ and $K^2 \times K^2$ dense matrices $(H_i^{\rm eff})_{kl}$ and $(V_{ij}^{\rm eff})_{kk'll'}$, respectively, can be written as a linear combination of at most $O[\mathrm{poly}(M)K^4]$ m-qubit Pauli operators, and hence can be estimated by $O[\mathrm{poly}(M)K^4]$ runs of quantum computers of m qubits. By minimizing the cost function, we obtain a better approximation of the ground state and its energy. One might think that the accuracy of estimating the matrix elements of $H^{\rm eff}$ would have a significant impact on the accuracy of the final energy, but this is not the case. According to a matrix perturbation theory, even if each element in a matrix has an additive error ϵ, the corresponding accuracy of the energy eigenvalue is bounded by $\mathrm{poly}(M)K^2\epsilon$. More precisely, suppose the estimated

Hamiltonian $\tilde{H}^{\text{eff}}$ is given by

$$\tilde{H}^{\text{eff}} = H^{\text{eff}} + H^{\text{error}}, \tag{19}$$

where the absolute value of each element of H^{error} is bounded by ϵ. Then the corresponding energy eigenvalues $\tilde{E}$ and E satisfy

$$|\tilde{E} - E| \leq \|H^{\text{error}}\|_\infty. \tag{20}$$

Since each term of H^{error} (and also $\tilde{H}^{\text{eff}}$) has a tensor product structure so as to act on at most K^2-dimensional subsystems. Therefore, we have

$$|\tilde{E} - E| \leq \|H^{\text{error}}\|_\infty \leq \text{poly}(M)K^2\epsilon. \tag{21}$$

Therefore, the accuracy can be guaranteed efficiently if ϵ is sufficiently small. Let $\bar{\epsilon}$ be a target accuracy of the energy. Then, ϵ should be

$$\epsilon = \frac{\bar{\epsilon}}{\text{poly}(M)K^2}, \tag{22}$$

and hence the number of measurements should be scaled $1/\epsilon^2 = \text{poly}(M)K^4/\bar{\epsilon}^2$.

Note that the proposed scheme shares an idea with Ref. [12] to estimate the effective Hamiltonian from the approximated ground state with local excitations. However, here we crucially put the step forward; the effective Hamiltonian is constructed including the interactions that are neglected when dividing the system into subsystems, and the effective Hamiltonian with reduced degrees of freedom is further solved by VQE at the second stage.

We also comment that instead of generating the local basis by a local excitation W_k, we can use subspace-search VQE to find an orthogonal basis of a low-energy subspace [13]. However, we find that this low-energy expansion results in worse energy than the above construction when the same number of dimensions of the local basis is employed. This might be attributed to the boundary error in the real-space renormalization as mentioned in Ref. [57]. Hopefully, the local excitations at the boundary can handle this issue, at least in a perturbative way as mentioned previously.

B. Multiple concatenations of VQE

In the above explanation, we concatenated VQE only twice. However, the procedure can be executed recursively to make a hierarchical structure to divide a larger problem into smaller pieces, where the correlations are taken like a real-space renormalization as shown in Fig. 2. Suppose a two-dimensional system is divided into multiple subsystems consisting of $l^{(1)} \times l^{(1)}$ qubits at the first level. After the first VQE, the local basis can be generated by the local excitations at the boundary. The dimensions of the local basis scale like $O(l^{(1)})$. Even if we take local excitations for all qubits including the bulk, the dimensions of the local basis are only $\text{poly}(l^{(1)})$. This means that, in the second level, the subsystem can be handled by $O[\log_2(l^{(1)})]$ qubits. By using the local basis, the effective Hamiltonian of the first level $H^{(1)}_{\text{eff}}$ is constructed including the intersubsystem interactions that are neglected in the first stage. In addition, we obtain the effective expression $\{W^{(1)}_{k,\text{eff}}\}$ of the local excitations at the boundary $\{W_k\}$, to generate the local basis in the next level.

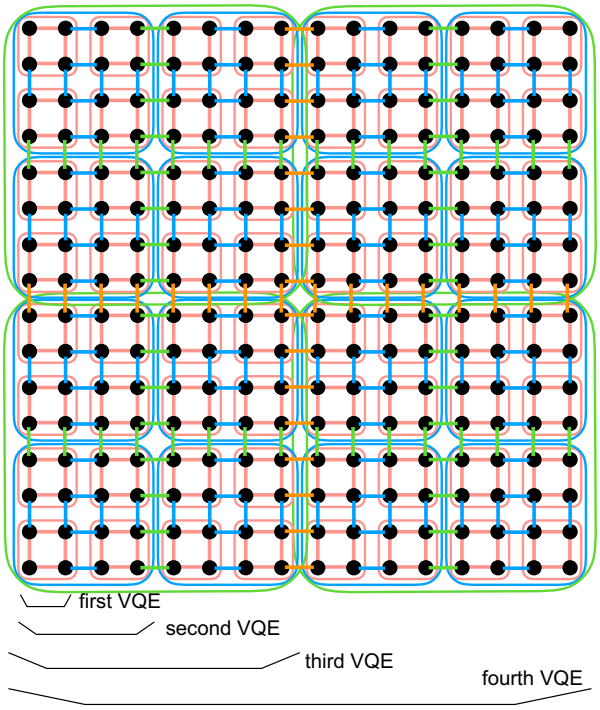

FIG. 2. Concatenation of VQEs. Red, blue, green squares correspond to the first, second, and third VQEs, respectively. The red, blue, green, and orange edges indicate the intersubsystem interactions taken at the first, second, third, and fourth VQEs. At each level, the local basis is generated by the local excitations on each qubit at the boundary, that is, the qubits engaged in the intersubsystem interactions. At each level, the effective Hamiltonian is constructed from suitably chosen local basis.

In the second level, we consider $l^{(2)} \times l^{(2)}$ lattice, each site of which is the system solved in the first VQE. The second VQE requires only $O[(l^{(2)})^2 \log(l^{(1)})]$ qubits. The local basis is generated by applying the local excitations $\{W^{(1)}_{k,\text{eff}}\}$ at the boundary of each subsystem in the second level. The dimensions of the local basis, i.e., the number of local excitations, are proportional to the length $O(l^{(1)}l^{(2)})$ of the boundary at the lowest level. By using the second-level local basis, the effective Hamiltonians and local excitations are constructed similarly.

By recursively repeating this procedure, at the $(k-1)$th level, the state obtained by the $(k-1)$th VQE is used to

generate a local basis. The length of the boundary at the lowest level is

$$l_{k-1} \equiv \prod_{j=1}^{k-1} l^{(j)}, \tag{23}$$

and hence the dimensions of the local basis are poly(l_{k-1}). By using the local basis, the effective Hamiltonian and local excitations at the kth level is obtained. At the kth-level concatenation, $l^{(k)} \times l^{(k)}$ lattice, where each site corresponds to the system spanned by the local basis in the $(k-1)$th level, is solved by kth VQE. The number of qubits required in the kth level is $O[(l^{(k)})^2 \log(l_{k-1})]$. Since the number of qubits handled at the lowest level increases exponentially in the number of concatenation k, it is enough to choose k as a logarithmic function of the problem size, i.e., the total number of physical qubits M. Then the total number of runs of quantum computers is only a polynomial in the problem size M. The number of qubits required is only logarithmic, $O[(l_{\max})^2 \log(M)]$, in the problem size M, where $l_{\max} = \max_k l^{(k)}$ is chosen to be a constant. In principle, this procedure can accommodate entanglement entropy scaling like $O[\log(|\partial D|)]$, where $|\partial D|$ is the length of the boundary of a region D.

In Fig. 2, we show the case with $l^{(k)} = 2$, where concatenation is performed up to $k = 4$ with a periodic boundary condition. Suppose three types of local excitations, for example, corresponding to the Pauli operators, are introduced on each qubit at the boundary. The dimensions of the local bases are $K = 13$, 37, and 85 at the second, third, and fourth level, respectively, which means that we should use 4, 6, and 7 qubits to represent each subsystem. In this case, 4, 16, 24, and 28 qubits in total are employed in each of first, second, third, and fourth VQEs, respectively. The total number of physical qubits is 256. If we add one more concatenation, a square lattice of length 32, i.e., 1024-qubit systems can be handled with 32-qubit quantum computers.

III. NUMERICAL SIMULATION

A. Quasi-one-dimensional systems

To make the proposed scheme more concrete, we demonstrate a series of numerical simulations. Numerical simulations are done by using Qulacs, an open-source fast quantum computer simulator on classical computers [58]. First, we consider the case where each local subsystem is governed by a four-qubit Heisenberg antiferromagnetic model:

$$H_i = \sum_{(\mu,\nu)\in E} (X_\mu^{(i)} X_\nu^{(i)} + Y_\mu^{(i)} Y_\nu^{(i)} + Z_\mu^{(i)} Z_\nu^{(i)}), \tag{24}$$

where the Pauli operator $A_\mu^{(i)}$ with $A \in \{X, Y, Z\}$ indicates the Pauli operator acting on the μth qubit in subsystem i, and $E = \{(0,1),(1,2),(2,3),(3,0),(0,2)\}$ is a set of edges. The whole system consists of N such subsystems that are coupled in a one-dimensional way via a Heisenberg antiferromagnetic interaction as shown in Fig. 3(a):

$$V_{ij} = X_0^{(i)} X_2^{(j)} + Y_0^{(i)} Y_2^{(j)} + Z_0^{(i)} Z_2^{(j)}, \tag{25}$$

where the 0th qubit in the ith subsystem and the second qubit in the j th subsystem are engaged in the interaction.

The parameterized quantum circuit is constructed as follows. For each cycle, we apply an arbitrary single-qubit gate on each qubit followed by a two-qubit gate generated

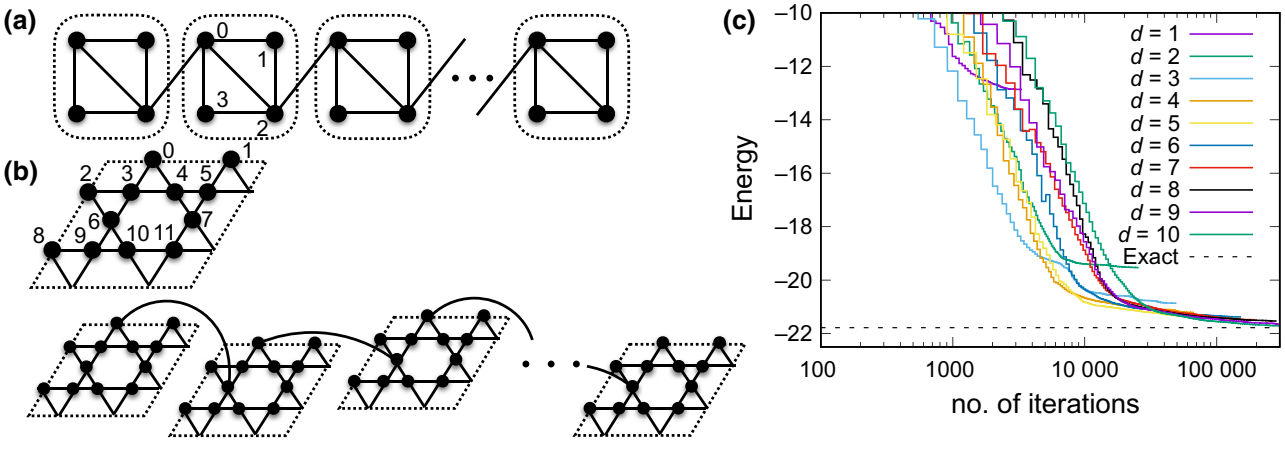

FIG. 3. (a) The system used for the numerical demonstration. It consists of four-qubit subsystems of Hamiltonian H_i, each of which interacts with each other by intersubsystem interaction V_{ij}. (b) A unit cell of Heisenberg antiferromagnetic model on a 12-qubit kagome lattice. The 12-qubit systems interact with each other in a nearest-neighbor way. (c) The energy obtained by the first VQE for the 12-qubit Heisenberg antiferromagnetic model. d indicates the depth, i.e., the number of cycles, of the parameterized quantum circuits. See Table I for the converged energies with increasing the ansatz depth.

TABLE I. Convergence of the energy for 12-qubit kagome lattice with increasing ansatz depth.

Depth d	1	2	3	4	5	6	7	8	9	10
energy	−12.86	−19.53	−20.96	−21.21	−21.43	−21.38	−21.48	−21.53	−21.65	−21.72

by the Heisenberg interaction

$$X_\mu X_\nu + Y_\mu Y_\nu + Z_\mu Z_\nu,$$

on each edge in E in a certain order. The cycle is repeated several times. The rotational angles with respect to the Pauli operators and the Heisenberg interactions are treated as the parameters of single-qubit and two-qubit gates, respectively. The parameters are optimized by using Broyden-Fletcher-Goldfarb-Shanno (BFGS) by using numerical differentiation. In an actual experiment, the gradient of the parameters should be obtained by using the parameter shift rule [59]. The exact ground-state energy of H_i is -7.0. The VQE with two cycles provides us an exact ground state $|\psi_0^{(i)}\rangle$ with the energy of -7.0 with the fidelity 1.0. This allows us to separate the performance analysis of the proposed scheme below from the imperfection of VQE at the first stage. Then, in addition to $|\psi_0^{(i)}\rangle$, we generate a local basis by the Pauli operators engaged in the intersubsystem interactions:

$$\{|\psi_0^{(i)}\rangle, A_0^{(i)}|\psi_0^{(i)}\rangle, \quad A_2^{(i)}|\psi_0^{(i)}\rangle\}. \tag{26}$$

In this case, the dimension of the local basis is $K = 7$, which can be treated with three qubits. While the dimensional reduction is not so large in this case, we regard this task as a validation of the proposed scheme. We calculate the effective Hamiltonian H^{eff} and solve it again with the VQE. In the second VQE, we use a parameterized quantum circuit, which is constructed of a single-subsystem unitary gate generated by the effective subsystem Hamiltonian H_i^{eff} and two-subsystem unitary gate generated by V_{ij}^{eff} with their rotational angles are taken as the following parameters:

$$U(\vec{\phi}) \equiv \prod_l W_l(\vec{\phi}^{(l)}), \tag{27}$$

$$W_l(\vec{\phi}^{(l)}) \equiv \prod_i e^{-i\phi_i^{(l)} H_i^{\text{eff}}} \prod_{\langle jk\rangle} e^{-i\phi_{jk}^{(l)} V_{jk}^{\text{eff}}}, \tag{28}$$

where the product $\prod_{\langle jk\rangle}$ runs over subsystems interacting with inter-subsystem interactions. Note that these gates, $e^{-i\phi_i^{(l)} H_i^{\text{eff}}}$ and $e^{-i\phi_{jk}^{(l)} V_{jk}^{\text{eff}}}$, are the $\lceil \log(K)\rceil$-qubit and $\lceil \log_2(K^2)\rceil$-qubit gate, respectively. Such unitary gates can be compiled from elementary single-qubit gates and two-qubit gates by Solovay-Kitaev algorithm or variational quantum gate optimization [60]. These work efficiently, since K is chosen to be at most polynomially large in the problem size n.

The results are summarized in Table II, where the energy expectation value calculated from the product state of the local ground state $|\psi_0\rangle^{\otimes N}$, the exact ground energy for H^{eff}, and the exact ground-state energy of H estimated by the Lanczos method on Qulacs or QS^3 are also shown as a comparison. In the case of $N = 2$, the proposed method provides the almost exact ground state. In the case of $3 \le N \le 8$, the obtained energies are 0.1%–0.4% higher than the exact energy obtained by the Lanczos method. This is attributed to the fact that the local basis employed to expand H^{eff} is not enough to achieve an exact ground-state energy, since VQE at the second stage successfully provides the ground state of H^{eff}. In all cases, we can see that the proposed scheme provides a better approximation of the ground-state energy smaller than those obtained by local ground states, i.e., H_{00}^{eff}. This implies that an entangled state of local basis states is generated to reduce the total energy.

In the above example, the effect of dimensional reduction is small. Next, we consider a tougher example, where each local subsystem is a Heisenberg antiferromagnetic model with a 12-qubit kagome lattice, as shown in Fig. 3(b). The parameterized quantum circuit is constructed in the same way as the previous case. The first VQE with depth 10 for the 12-qubit subsystem results in a good approximation -21.72 of the exact ground-state energy -21.78, which corresponds to fidelity 0.977 as shown in Fig. 3(c) and Table I. The intersubsystem interactions are introduced so that the 12-qubit subsystems interact in a one-dimensional way. Specifically, zeroth and sixth qubits, each of which belongs to neighboring subsystems, interact with the Heisenberg antiferromagnetic interaction.

TABLE II. Numerical results for $4 \times N$ Heisenberg antiferromagnetic systems shown in Fig. 3(a). "Deep VQE" indicates the results obtained by the proposed scheme. "Local" indicates the energy calculated from a product state of the local ground state $|\psi_0\rangle$, i.e., H_{00}^{eff}. "Effective" means the exact ground-state energy of H^{eff}. "Exact" is a ground-state energy calculated by Lanczos method on a simulator; the exact energy for the 4×8 system is computed by use of a quantum spin solver QS^3 [61].

System	Deep VQE	Local	Effective	Exact
4×2	−14.46	−14.00	−14.46	−14.46
4×3	−21.89	−21.00	−21.89	−21.92
4×4	−29.31	−28.00	−29.32	−29.39
4×5	−36.70	−35.00	−36.75	−36.85
4×6	−44.13	−42.00	NA	−44.31
4×8	−59.02	−56.00	NA	−59.23

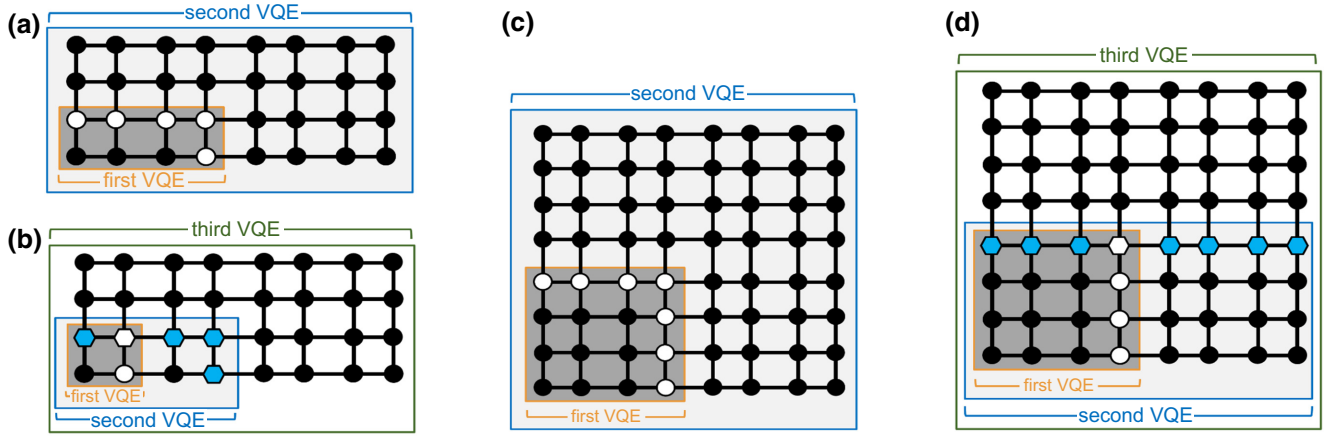

FIG. 4. The protocol of concatenating of VQEs employed in the numerical demonstration of 2D systems. Qubits marked by white symbols are located at the boundary of subsystems for the first VQE. Hexagons (both blue and white) indicate the boundary sites of subsystems for the second VQE, which are used for constructing the local basis following Eq. (31). (a) 32 sites with the concatenation up to the second VQE. (b) 32 sites with the concatenation up to the third VQE. (c) 64 sites with the concatenation up to the second VQE. (d) 64 sites with the concatenation up to the third VQE.

The local basis is generated in the same way as the previous example. This means that we approximate the 12-qubit system as a seven-dimensional system, i.e., three qubits, and hence the dimensional reduction enabled by the proposed method is apparent. The ansatz for the second VQE is again constructed in the same way as the previous case.

In the case of $N = 2$ and 4, i.e., two and four subsystems, respectively, the proposed method results in energy -43.8 and -87.9, both of which achieve the exact ground-state energy of the effective Hamiltonians. In the case of $N = 2$, the Lanczos method provides -44.055 and the deep VQE works well while reducing the total number of qubits. While in the case of $N = 4$ we cannot compare the result with the exact energy obtained by the Lanczos method , at least we can say that the energy obtained is smaller than the energy expectation value $H_{00}^{\text{eff}} = -43.4$ and $H_{00}^{\text{eff}} = -86.9$ estimated by a product state of the local ground state $|\psi_0\rangle$. In this case, the problem of the 48-qubit system is solved using VQEs with 12 qubits, which are feasible within the current technology. The accuracy would be improved by appending more states to the local basis. Even if the dimensions of the local basis are doubled, it only results in adding one more qubit to each site in the second VQE.

B. Two-dimensional systems

We also demonstrate the performance of deep VQE and the further concatenated VQE for two-dimensional (2D) systems, which give rise to larger reduction of qubits. We consider a Heisenberg antiferromagnetic model on a 2D $(L_x \times L_y)$-site square lattice, whose Hamiltonian is

$$H = \sum_{\{\mu,\nu\}\in E} (X_\mu X_\nu + Y_\mu Y_\nu + Z_\mu Z_\nu). \tag{29}$$

The set of edges E is composed of pairs of neighboring sites under the open boundary condition. Assuming that both L_x and L_y are finite and even, this model has a unique ground state respecting the SU(2) symmetry.

We examine our protocol up to the second VQE on a 16-qubit system with $L_x = 4, L_y = 4$. We choose each subsystem for the 1st VQE by a (2×2)-site lattice (see Fig. 2). The first VQE is performed by a hardware-efficient ansatz with depth 10, reproducing the exact ground-state energy of each subsystem, -8.00. The local basis is chosen by $\{|\psi_0^{(i)}\rangle, A_\mu^{(i)}|\psi_0^{(i)}\rangle\}$, where we take a site μ from the boundary of the ith subsystem. With the local dimension $K = 10$, the second VQE requires 16 qubits. Although the number of required qubits does not decreases here, note that the information of the whole Hilbert space is abandoned at the rate of 0.85. We calculate the exact energy of H^{eff} instead of performing the second VQE due to the computational cost. The resulting ground-state energy is -36.43, which well reproduces the Lanczos result -36.76 compared to the energy expectation value $H_{00}^{\text{eff}} = -32.00$.

Let us discuss the concatenation up to the third VQE for larger 2D systems, which are difficult to classically simulate. We pick up 32-qubit $(L_x = 8, L_y = 4)$ or 64-qubit $(L_x\ L_y = 8)$ systems described by the Heisenberg Hamiltonian Eq. (29). We show the subsystems at each step in Figs. 4(b) and 4(d). For the 32-qubit system, we consider two different choices of the local basis. After the first VQE on each four-qubit subsystem, the local excitation operators $\{W_k^{(i)}\}_{k=1}^K$ are chosen from the identity and the Pauli operators at the boundary connected to other subsystems $(K = 7)$, leading to the second VQE on the six effective qubits. Next, we introduce two local operator sets:

$$\text{(A): } \{I, X_{\mu^{\text{eff}}}^{(i)}, Y_{\mu^{\text{eff}}}^{(i)}, Z_{\mu^{\text{eff}}}^{(i)}\}, \tag{30}$$

TABLE III. Numerical results for 2D Heisenberg antiferromagnetic systems. "Deep VQE" indicates the results obtained by the proposed scheme. "$\mathcal{W}_{\text{second}}$" designates the set of local excitations from Eqs. (30) and (31) when we iterate up to the third VQE. "Local" is given by H_{00}^{eff} where H^{eff} is the effective Hamiltonian used for the last VQE in the protocol. "Effective" means the deep VQE results of the ground-state energy under the assumption that VQEs are accurate enough, calculated by replacing the VQEs by the exact diagonalization."Exact" means a ground-state energy obtained by the Lanczos method on the quantum spin simulator QS^3[61] except for 64 sites, where –158.47* is obtained by the looper quantum Monte Carlo codes in ALPS [62,63]. "Qubits" indicates the number of qubits required through the protocol.

System	Order	$\mathcal{W}_{\text{second}}$	Local	Effective	Exact	Qubits
16 sites	Second	—	−32.00	−36.43	−36.76	16
32 sites (8×4)	Second	—	−68.69	−74.60	−76.30	16
	Third	(A)	−68.55	−69.57		20
		(B)	−68.55	−71.49		16
64 sites (8×8)	Second	—	−147.03	−153.11	−158.47*	20
	Third	(B)	−149.61	−151.39		16

where μ^{eff} runs over the six effective qubits ($K = 19$), or

$$\text{(B)}: \{I, X^{(i)}_{\mu,\text{eff}}, Y^{(i)}_{\mu,\text{eff}}, Z^{(i)}_{\mu,\text{eff}}\}, \tag{31}$$

where μ runs over the original boundary qubits connected to other subsystems ($K = 16$). Note that $A_{\nu,\text{eff}}$ ($A = X, Y, Z$) physically represents the Pauli operator A_ν in the original system, but we should compute its matrix elements in the new basis for the effective model after the first VQE. Considering the result for the 32-qubit system discussed later, we construct the local basis by Eq. (31) after the second VQE for the 64-qubit system ($K = 25$).

Table III shows the numerical results for the 2D systems. To evaluate the performance of the concatenated VQE with reducing the computational cost, we replace the VQEs by the exact diagonalization. We confirm that, for the 32-qubit system, the first and the second VQEs with hardware-efficient ansatz can reproduce the exact ground states of the corresponding subsystems with fidelity 1.000 and 0.998, respectively, indicating the validity of this replacement for assessing the deep VQE results. We also simulate the concatenation up to the second VQE in the way of Figs. 4(a) and 4(c) to compare the results. For the 32-qubit system, while the third VQE results are worse than that of the second VQE due to repeated coarse-graining, they give approximate ground-state energy −69.57 [for the local basis with (A)] and −71.49 [for the one with (B)], reproducing the exact result −76.30 better than the local result −68.55.

Let us discuss why the local basis choice (B) gives a better result than (A) to identify the better choice of the local basis when considering larger systems or further concatenation of VQEs. For the third VQE, we employ the effective Hamiltonian after the second VQE as a Hamiltonian of each subsystem. Since the effective Hamiltonian is generally nonlocal within each subsystem, it is difficult to describe excitations within each subsystem by a set of local operators. In our simulation for the 32-qubit system, the choice (A) captures local excitations in each subsystem while the choice (B) captures excitations that are local in the original system but nonlocal in each subsystem after the second VQE. The better result of the choice (B) implies that the picture of linear excitations at the boundaries is maintained through the coarse graining, and hence choosing the local excitation operators at the boundaries based on the original lattice is suitable also for further-concatenated VQEs or for larger systems. Based on this, we also simulate the 64-qubit system with the local basis choice by (B). We obtain the second VQE result 153.11 and the third VQE result −151.39, and both of them well reproduce the approximate value −158.47 computed by the looper quantum Monte Carlo codes in ALPS [62,63]. While the concatenation up to the third VQE gives a slightly worse upper bound for the ground-state energy than the second VQE result, we can efficiently complete the simulation with further decreasing the size of quantum devices by four qubits.

A better upper bound of the ground-state energy or equivalently a more accurate value will be achieved if we consider local excitations near the boundaries of subsystems or higher-order excitations when constructing the local basis also in two-dimensional systems, keeping the merit of decrease in qubits. Since low-entangled states in higher-dimensional systems are difficult to classically simulate by matrix-product-state-based methods such as the density-matrix renormalization group [57], the concatenation of VQEs will significantly benefit us in simulating classically intractable higher-dimensional systems.

IV. CONCLUSION AND DISCUSSION

We have proposed a DC method for the quantum-classical hybrid algorithm to solve a larger system with a small size of quantum computers. Specifically, VQE is performed recursively to reduce the physical dimensions, while taking the interactions via the effective Hamiltonian. Though we have considered only quasi-one-dimensional

and two-dimensional Heisenberg anti-ferromagnetic models in the numerical simulations, the proposed scheme is applicable to more complicated systems such as complex molecules such as molecular aggregates, molecular crystals, and dendrimers. If the subsystem is a strongly correlated system, which inevitably requires a highly entangled state available only by quantum computers, the proposed scheme allows us to use quantum computers of relatively small size for large enough problems.

As a future direction, the proposed scheme can be hybridized with the classical tensor network approaches so that the effective Hamiltonian obtained from the first VQE can be solved by using tensor-network methods as reported in Refs. [64,65]. More precisely, in Ref. [65], the authors have proposed various types of quantum-classical hybrid tensor network models. For example, if we employ a MPS ansatz classically after the first VQE in our proposal, then it can be seen as a connection of classical and quantum tensor networks mentioned in Ref. [65]. Furthermore, the deep VQE, i.e., concatenation of VQEs at multiple stages is similar to the quantum-quantum tensor network in Ref. [65]. Specifically, if we employ the subspace search VQE to span a low-energy subspace, we have the same structure of tree type as that in Ref. [65]. However, the local excitations and Schmidt process to span local bases cannot be regarded as a simple connection between two quantum tensor networks via classical tensor. Therefore it is useful for a quantum-classical hybrid tensor network to enhance its performance further by introducing a nontrivial classical processing on a classical part connecting different quantum tensors.

Note that, one of the reasons why the deep VQE works well for the ground-state analysis of the $d(=1,2)$-dimensional antiferromagnetic Heisenberg model, despite introducing a dramatic reduction of degrees of freedom, is that the degrees of freedom K for a local cluster automatically increases proportionally to the surface area of the cluster $O(\ell^{d-1})$ where ℓ is the length of one side of the cluster. We should emphasize that such area law of space expansion employed in the deep VQE partially incorporates the property of entropic area law [66] for a d-dimensional quantum many-body system consisting only of short-range interactions that the entanglement entropy is proportional to the surface area $O(l^{d-1})$ of the subsystem. One guiding principle for deepening the deep VQE based of the entropic area law is to develop a procedure that controls the number of local degrees of freedom of the cluster to be increased by an arbitrary order of integer power with respect to its surface area, so that as a extreme case of the procedure the local degrees of freedom can be increased by $O[\exp(l^{d-1})]$ satisfying the entropic area law. For example, taking into account an effect of a $n(>1)$th-order perturbation, it would be a naive extension of the deep VQE to prepare a local degree of freedom proportional to the nth power of the surface area by letting the n bodies Pauli products act on the qubits near the interface with respect to the ground state of the cluster. The validity of such an extension originating from this work is one of the future issues.

ACKNOWLEDGMENTS

K.F. is supported by JST ERATO JPMJER1601, and JST CREST JPMJCR1673. This work is supported by MEXT Quantum Leap Flagship Program (MEXT Q-LEAP) Grant No. JPMXS0118067394 and JPMXS0120319794, and JST COI-NEXT Grant No. JPMJPF2014. Kaoru Mizuta appreciates the support of WISE Program from MEXT and a Reseach Fellowship for Young Scientists from JSPS (Grant No. 20J12930). W.M. wishes to thank JSPS KAKENHI Grant No. 18K14181 and JST PRESTO Grant No. JPMJPR191A. H.U. is supported by KAKENHI Grants No. 17K1435, No. 21H04446, and No. 21H05191, and JST PRESTO Grant No. JPMJPR1911, and the COE research grant in computational science from Hyogo Prefecture and Kobe City through Foundation for Computational Science. We are grateful for allocating computational resources of the HOKUSAI BigWaterfall supercomputing system at RIKEN.

[1] P. W. Shor, Polynomial-time algorithms for prime factorization and discrete logarithms on a quantum computer, SIAM J. Comput. **26**, 1484 (1997).
[2] A. Aspuru-Guzik, Simulated quantum computation of molecular energies, Science **309**, 1704 (2005).
[3] S. McArdle, S. Endo, A. Aspuru-Guzik, S. C. Benjamin, and X. Yuan, Quantum computational chemistry, Rev. Mod. Phys. **92**, 015003 (2020).
[4] A. W. Harrow, A. Hassidim, and S. Lloyd, Quantum Algorithm for Linear Systems of Equations, Phys. Rev. Lett. **103**, 150502 (2009).
[5] A. M. Childs, R. Kothari, and R. D. Somma, Quantum algorithm for systems of linear equations with exponentially improved dependence on precision, SIAM J. Comput. **46**, 1920 (2017). .
[6] A. Gilyén, Y. Su, G. H. Low, and N. Wiebe, in *Proceedings of the 51st Annual ACM SIGACT Symposium on Theory of Computing - STOC 2019* (ACM Press, 2019).
[7] F. Arute *et al.*, Quantum supremacy using a programmable superconducting processor, Nature **574**, 505 (2019).
[8] J. Preskill, Quantum computing in the NISQ era and beyond, Quantum **2**, 79 (2018).
[9] A. Bouland, B. Fefferman, C. Nirkhe, and U. Vazirani, On the complexity and verification of quantum random circuit sampling, Nat. Phys. **15**, 159 (2018).
[10] S. Boixo, S. V. Isakov, V. N. Smelyanskiy, R. Babbush, N. Ding, Z. Jiang, M. J. Bremner, J. M. Martinis, and H. Neven, Characterizing quantum supremacy in near-term devices, Nat. Phys. **14**, 595 (2018).

[11] A. Peruzzo, J. McClean, P. Shadbolt, M.-H. Yung, X.-Q. Zhou, P. J. Love, A. Aspuru-Guzik, and J. L. O'Brien, A variational eigenvalue solver on a photonic quantum processor, Nat. Commun. **5**, 4213 (2014).

[12] J. R. McClean, M. E. Kimchi-Schwartz, J. Carter, and W. A. de Jong, Hybrid quantum-classical hierarchy for mitigation of decoherence and determination of excited states, Phys. Rev. A **95**, 042308 (2017).

[13] K. M. Nakanishi, K. Mitarai, and K. Fujii, Subspace-search variational quantum eigensolver for excited states, Phys. Rev. Res. **1**, 033062 (2019).

[14] O. Higgott, D. Wang, and S. Brierley, Variational quantum computation of excited states, Quantum **3**, 156 (2019).

[15] R. M. Parrish, E. G. Hohenstein, P. L. McMahon, and T. J. Martínez, Quantum Computation of Electronic Transitions Using a Variational Quantum Eigensolver, Phys. Rev. Lett. **122**, 230401 (2019).

[16] T. Jones, S. Endo, S. McArdle, X. Yuan, and S. C. Benjamin, Variational quantum algorithms for discovering Hamiltonian spectra, Phys. Rev. A **99**, 062304 (2019).

[17] N. Yoshioka, Y. O. Nakagawa, K. Mitarai, and K. Fujii, Variational quantum algorithm for non-equilibrium steady states, Phys. Rev. Res. **2**, 043289 (2020).

[18] K. Mitarai, Y. O. Nakagawa, and W. Mizukami, Theory of analytical energy derivatives for the variational quantum eigensolver, Phys. Rev. Res. **2**, 013129 (2020).

[19] R. M. Parrish, E. G. Hohenstein, P. L. McMahon, and T. J. Martinez, Hybrid quantum/classical derivative theory: Analytical gradients and excited-state dynamics for the multistate contracted variational quantum eigensolver, arXiv:1906.08728 [quant-ph] (2019).

[20] T. E. O'Brien, B. Senjean, R. Sagastizabal, X. Bonet-Monroig, A. Dutkiewicz, F. Buda, L. DiCarlo, and L. Visscher, Calculating energy derivatives for quantum chemistry on a quantum computer, Npj Quantum Inf. **5**, 113 (2019).

[21] K. Temme, S. Bravyi, and J. M. Gambetta, Error Mitigation for Short-Depth Quantum Circuits, Phys. Rev. Lett. **119**, 180509 (2017).

[22] S. Endo, S. C. Benjamin, and Y. Li, Practical Quantum Error Mitigation for Near-Future Applications, Phys. Rev. X **8**, 031027 (2018).

[23] P. Czarnik, A. Arrasmith, P. J. Coles, and L. Cincio, Error mitigation with clifford quantum-circuit data, Quantum **5**, 592 (2021).

[24] A. Strikis, D. Qin, Y. Chen, S. C. Benjamin, and Y. Li, Learning-based quantum error mitigation, PRX Quantum **2**, 040330 (2021).

[25] R. Takagi, Optimal resource cost for error mitigation, Phys. Rev. Res. **3**, 033178 (2021).

[26] Z. Cai, Multi-exponential error extrapolation and combining error mitigation techniques for nisq applications, npj Quantum Inf **7**, 80 (2021).

[27] A. Kandala, K. Temme, A. D. Córcoles, A. Mezzacapo, J. M. Chow, and J. M. Gambetta, Error mitigation extends the computational reach of a noisy quantum processor, Nature **567**, 491 (2019).

[28] K. Mitarai and K. Fujii, Constructing a virtual two-qubit gate from single-qubit operations, New J. Phys. **23**, 023021 (2021).

[29] K. Mitarai and K. Fujii, Overhead of the non-local-to-local channel decomposition by quasiprobability sampling, Quantum **5**, 388 (2021).

[30] T. Peng, A. Harrow, M. Ozols, and X. Wu, Simulating large quantum circuits on a small quantum computer, Phys. Rev. Lett. **125**, 150504 (2020).

[31] S. Bravyi, J. M. Gambetta, A. Mezzacapo, and K. Temme, Tapering off qubits to simulate fermionic hamiltonians, arXiv:1701.08213 [quant-ph] (2017).

[32] K. Setia, R. Chen, J. E. Rice, A. Mezzacapo, M. Pistoia, and J. Whitfield, Reducing qubit requirements for quantum simulation using molecular point group symmetries, J. Chem. Theory Comput. **16**, 6091 (2020).

[33] J. Romero, R. Babbush, J. R. McClean, C. Hempel, P. J. Love, and A. Aspuru-Guzik, Strategies for quantum computing molecular energies using the unitary coupled cluster ansatz, Quantum Sci. Technol. **4**, 014008 (2018).

[34] W. Mizukami, K. Mitarai, Y. O. Nakagawa, T. Yamamoto, T. Yan, and Y. ya Ohnishi, Orbital optimized unitary coupled cluster theory for quantum computer, Phys. Rev. Research **2**, 033421 (2020).

[35] T. Takeshita, N. C. Rubin, Z. Jiang, E. Lee, R. Babbush, and J. R. McClean, Increasing the Representation Accuracy of Quantum Simulations of Chemistry without Extra Quantum Resources, Phys. Rev. X **10**, 011004 (2020).

[36] W. Yang and T.-S. Lee, A density-matrix divide-and-conquer approach for electronic structure calculations of large molecules, J. Chem. Phys. **103**, 5674 (1995).

[37] M. S. Gordon, D. G. Fedorov, S. R. Pruitt, and L. V. Slipchenko, Fragmentation methods: A route to accurate calculations on large systems, Chem. Rev. **112**, 632 (2012).

[38] C. A. Jiménez-Hoyos and G. E. Scuseria, Cluster-based mean-field and perturbative description of strongly correlated fermion systems: Application to the one- and two-dimensional Hubbard model, Phys. Rev. B **92**, 085101 (2015).

[39] M. R. Hermes and L. Gagliardi, Multiconfigurational self-consistent field theory with density matrix embedding: The localized active space self-consistent field method, J. Chem. Theory Comput. **15**, 972 (2019).

[40] M. R. Hermes, R. Pandharkar, and L. Gagliardi, Variational localized active space self-consistent field method, J. Chem. Theory Comput. **16**, 4923 (2020).

[41] H. Wang and M. Thoss, Multilayer formulation of the multiconfiguration time-dependent hartree theory, J. Chem. Phys. **119**, 1289 (2003).

[42] H.-D. Meyer and G. A. Worth, Quantum molecular dynamics: Propagating wavepackets and density operators using the multiconfiguration time-dependent hartree method, Theor. Chem. Acc. **109**, 251 (2003).

[43] S. M. Parker, T. Seideman, M. A. Ratner, and T. Shiozaki, Communication: Active-space decomposition for molecular dimers, J. Chem. Phys. **139**, 021108 (2013).

[44] S. Parker and T. Shiozaki, Communication: Active space decomposition with multiple sites: Density matrix renormalization group algorithm, J. Chem. Phys. **141**, 211102 (2014).

[45] S. Nishio and Y. Kurashige, Rank-one basis made from matrix-product states for a low-rank approximation of molecular aggregates, J. Chem. Phys. **151**, 084110 (2019).

[46] H. Nakano and K. Hirao, A quasi-complete active space self-consistent field method, Chem. Phys. Lett. **317**, 90 (2000).

[47] M. Al Hajj, J.-P. Malrieu, and N. Guihéry, Renormalized excitonic method in terms of block excitations: Application to spin lattices, Phys. Rev. B **72**, 224412 (2005).
[48] H. Zhang, J.-P. Malrieu, H. Ma, and J. Ma, Implementation of renormalized excitonic method at ab initio level, J. Comput. Chem. **33**, 34 (2012).
[49] N. J. Mayhall, Large-scale variational two-electron reduced-density-matrix-driven complete active space self-consistent field methods, J. Chem. Theory Comput. **13**, 4818 (2017).
[50] V. Abraham and N. J. Mayhall, Selected configuration interaction in a basis of cluster state tensor products, J. Chem. Theory Comput. **16**, 6098 (2020).
[51] T. Yamazaki, S. Matsuura, A. Narimani, A. Saidmuradov, and A. Zaribafiyan, Towards the practical application of near-term quantum computers in quantum chemistry simulations: A problem decomposition approach, arXiv:1806.01305 [quant-ph] (2018).
[52] N. C. Rubin, arXiv preprint arXiv:1610.06910 (2016).
[53] G. Knizia and G. K.-L. Chan, Density Matrix Embedding: A Simple Alternative to Dynamical Mean-Field Theory, Phys. Rev. Lett. **109**, 186404 (2012).
[54] R. Nagata, H. Nakanotani, W. J. Potscavage Jr, and C. Adachi, Exploiting singlet fission in organic light-emitting diodes, Adv. Mater. **30**, 1801484 (2018).
[55] D. Casanova, Theoretical modeling of singlet fission, Chem. Rev. **118**, 7164 (2018).
[56] S. J. Jang and B. Mennucci, Delocalized excitons in natural light-harvesting complexes, Rev. Mod. Phys. **90**, 035003 (2018).
[57] U. Schollwöck, The density-matrix renormalization group, Rev. Mod. Phys. **77**, 259 (2005).
[58] Y. Suzuki, Y. Kawase, Y. Masumura, Y. Hiraga, M. Nakadai, J. Chen, K. M. Nakanishi, K. Mitarai, R. Imai, and S. Tamiya *et al.*, Qulacs: a fast and versatile quantum circuit simulator for research purpose, Quantum **5**, 559 (2021).
[59] K. Mitarai, M. Negoro, M. Kitagawa, and K. Fujii, Quantum circuit learning, Phys. Rev. A **98**, 032309 (2018).
[60] K. Heya, Y. Suzuki, Y. Nakamura, and K. Fujii, Variational quantum fate optimization, arXiv preprint arXiv:1810.12745 (2018).
[61] H. Ueda, S. Yunoki, and T. Shimokawa, Quantum spin solver near saturation: QS^3, arXiv e-prints, arXiv:2107.00872 (2021).
[62] A. Albuquerque *et al.*, The ALPS project release 1.3: Open-source software for strongly correlated systems, J. Magn. Magn. Mater. **310**, 1187 (2007), proceedings of the 17th International Conference on Magnetism.
[63] B. Bauer *et al.*, The ALPS project release 2.0: Open source software for strongly correlated systems, J. Stat. Mech.: Theory Exp. **2011**, P05001 (2011).
[64] J.-G. Liu, Y.-H. Zhang, Y. Wan, and L. Wang, Variational quantum eigensolver with fewer qubits, Phys. Rev. Res. **1**, 023025 (2019).
[65] X. Yuan, J. Sun, J. Liu, Q. Zhao, and Y. Zhou, Quantum Simulation with Hybrid Tensor Networks, Phys. Rev. Lett. **127**, 040501 (2021).
[66] P. Calabrese and J. Cardy, Entanglement entropy and quantum field theory, J. Stat. Mech.: Theory and Exp. **2004**, P06002 (2004).